1 # Classification of Large-Scale Environments that drive the formation
2 # of Mesoscale Convective Systems over Southern West Africa

3

4 Francis Nkrumah[1,2], Cornelia Klein[3,5], Kwesi Akumenyi Quagraine[1,4], Rebecca Berkoh
5 Oforiwaa[2,6], Nana Ama Browne Klutse[2,6], Patrick Essien[1,2], Gandomè Mayeul Leger Davy
6 Quenum[2,7] and Hubert Azoda Koffi[6]

7

8 [1]Department of Physics, University of Cape Coast, Private Mail Bag, Cape Coast, Ghana;
9 [2]African Institute of Mathematical Sciences (AIMS), Sector Remera, Kigali 20093, Rwanda;
10 [3]U.K. Centre for Ecology and Hydrology, Wallingford, United Kingdom
11 [4]Climate System Analysis Group (CSAG), ENGEO, University of Cape Town, Private Bag X3, Rondebosch,
12 Cape Town 7701, South Africa
13 [5]Department of Atmospheric and Cryospheric Sciences, University of Innsbruck, Innsbruck, Austria
14 [6]Department of Physics, University of Ghana, Legon P.O. Box LG 63, Ghana
15 [7]National Institute of Water (NIW), University of Abomey-Calavi, Godomey, Cotonou 01 PB: 4521, Benin

16
17 *Correspondence to*: Francis Nkrumah (francis.nkrumah@ucc.edu.gh) and Nana Ama Browne Klutse
18 (nklutse@ug.edu.gh)

19

20 **Abstract.** Mesoscale convective systems (MCSs) are frequently observed over southern West Africa (SWA)
21 throughout most of the year. However, it has not yet been identified what variations in typical large-scale
22 environments of the West African monsoon seasonal cycle may favour MCS occurrence in this region. Here, six
23 distinct synoptic states are identified and are further associated with being either a dry season, pre-, post-, or peak-
24 monsoon synoptic circulation type using self organizing maps (SOMs) with inputs from reanalysis data. We
25 identified a pronounced annual cycle of MCS numbers with frequency peaks in June and September which can be
26 associated with peak rainfall during the major and minor rainy seasons respectively across SWA. Comparing daily
27 MCS frequencies, MCSs are most likely to develop during post-monsoon conditions featuring a northward-
28 displaced moisture anomaly (0.42 MCSs per day), which can be linked to strengthened low-level westerlies.
29 Considering that these post-monsoon conditions occur predominantly from September and into November, these
30 patterns may in some cases be representative of a delayed monsoon retreat. On the other hand, under peak monsoon
31 conditions, we observe easterly wind anomalies during MCS days, which reduce moisture content over the Sahel but
32 introduce more moisture over the coast. Finally, we find all MCS-day synoptic states to exhibit positive shear
33 anomalies. Seasons with the strongest shear anomalies are associated with the strongest low-level temperature
34 anomalies to the north of SWA, highlighting that a warmer Sahel can promote MCS-favourable conditions in SWA.
35 These significant positive zonal shear anomalies for MCS days illustrate the importance of shear for MCS
36 development in SWA throughout the year.

37 **1 Introduction**

38   The region of West Africa is subject to variabilities in rainfall on both spatial and temporal scales.
39 Fundamentally, the rainfall pattern in West Africa is modulated by the annual change in the position of the

40 Intertropical Convergence Zone (ITCZ) and the West African Monsoon (WAM). Due to endemic poverty, lack of
41 infrastructure and technology, rapid population increase, and significant fluctuation of the WAM, West Africa has
42 been deemed one of the world's most susceptible regions to climate change (Change, 2014). The climate of southern
43 West Africa (SWA) can be categorized into four seasonal stages: a dry season from December to February, two wet
44 seasons lasting from April to June, and September to November, and the so-called little dry season in August (e.g.
45 Thorncroft et al. 2011). Between March and June, when low-level winds are more westerly and the intertropical
46 convergence zone (ITCZ) starts to move northward, the precipitable water peaks over SWA (Klein et al. 2021). The
47 ITCZ retreats southward in September, creating the second rainy season, followed by a dry season from November
48 to January.

49   One of the most destructive high-impact weather phenomena in West and Central Africa are mesoscale
50 convective systems (MCSs), together with the precipitation, wind, and lightning they bring (Baidu et al. 2022).
51 MCSs are organized thunderstorm clusters, often defined to have a minimum horizontal extent of the precipitating
52 area of 100 kilometres in at least one direction (Guo et al. (2022); Chen et al. (2022); Houze (2004)). Maranan et al.
53 (2018) note that diverse MCS sub-groups such as squall- or disturbance lines, structured convective systems, and
54 mesoscale convective complexes impact the hydro-climate of West Africa. In both the tropics and midlatitudes,
55 MCS also contributes significantly to rainfall extremes, rendering them a substantial contributor to the hydrologic
56 cycle (Feng et al. (2021); Li et al. (2020)). More studies have been motivated in recent decades by evaluating drivers
57 that affect rainfall variability and intensity associated with MCSs (Baidu et al. (2022); Augustin et al. (2022)).
58 MCSs, for instance, supply essential precipitation and, as a result, supply water to agriculturally productive regions
59 in the tropics, particularly in semi-arid regions such as the Sahel (Nesbitt et al. (2006)).

60   However, relative to our understanding of MCS drivers in the Sahel, SWA has received less attention. The
61 connections of MCSs to larger-scale atmospheric motion and states are both important and not fully understood for
62 the southern region, hence, a better understanding of large-scale MCS drivers is important for improving
63 precipitation prediction over SWA. Earlier research has suggested an increasing role of other types of less-organized
64 rainfall in place of MCSs over the Guinea Coast (e.g. (Acheampong, 1982; Fink et al., 2006; Kamara, 1986;
65 Omotosho, 1985), with MCS contribution to annual rainfall decreasing from 71% in the Soudanian to 56% in the
66 coastal zone (Maranan et al 2018), emphasizing MCS importance across the SWA region. Maranan et al., 2018 also
67 concluded that precipitable water and Convective Available Potential Energy (CAPE) determine where MCSs may
68 occur in SWA, while wind shear is a stronger predictor for distinguishing between small scattered convection and
69 MCS-type development. Indeed, wind shear intensification was found to be a major driver of increasing frequencies
70 of the most intense Sahelian MCSs over the last three decades (Taylor et al., 2017), a mechanism that was similarly
71 found to play a role for early-season MCS intensification in SWA (Klein et al 2021). Wind shear, which is thought
72 to modulate the storm-available supply of moist buoyant air, is also seen to be very critical to the organization of
73 convective systems (e.g., Alfaro, 2017; Mohr & Thorncroft, 2006). Accordingly, propagating storms with longer-
74 lasting organized precipitation systems were consistently found to be associated with strong vertical wind shear and
75 higher values of CAPE in the Sahel (Hodges & Thorncroft, 1997; Laing et al., 2008; Mohr & Thorncroft, 2006).

76   In previous studies that evaluated MCS-favouring atmospheric environments, less attention was given to

77   the importance of large-scale WAM modes and their effect on regional MCS frequencies in SWA. The role of

78   regional MCS-centred environments in the initiation and development of MCSs in West Africa has been well

79   studied (e.g., Klein et al. 2021; Vizy and Cook 2018; Schrage et al. 2006; Maranan et al. 2018). Vizy and Cook

80   (2018) observed that the extension of vertical mixing to the level of free convection, as a result of surface heating,

81   tends to initiate MCSs in an environment where the mid-tropospheric African easterly wave disturbance is located in

82   the east. The vertical wind shear is enhanced as a result of the synoptic disturbance. Klein et al. (2021) suggested

83   that heavy rainfall, due to cold MCSs during both dry and rainy seasons, occurs in an environment with stronger

84   wind shear, increased low-level humidity, and drier mid-levels. Unlike vertical wind shear, Maranan et al., (2018)

85   suggested that thermodynamic conditions such as CAPE and Convective Inhibition (CIN) are of lesser importance

86   for the horizontal growth of convective systems, although they indicate the potential of the initial vertical

87   development of convective systems. Janiga and Thorncroft (2016) also suggested that CAPE, vertical wind shear

88   and column relative humidity are the decisive large-scale environments that control the characteristics of convective

89   systems. Based on radar and sounding observations aligned around 15°N, Guy et al. (2011) analyzed MCSs and their

90   respective environmental conditions over three different regimes of West Africa (maritime, coastal, and continental).

91   They concluded that MCSs tend to occur ahead of the African easterly wave (AEW) trough during the maritime and

92   the continental regime, while they are mostly found behind the trough in the coastal regime.

93   It is not clear to what extent different large-scale patterns at different stages of the WAM drive the

94   formation of MCSs over SWA. Hence, this study systematically classifies the different large-scale patterns across

95   the WAM region and how they are associated with MCSs over SWA. For this purpose, a classification using a self

96   organizing map (SOM; Kohonen 2001) analysis was carried out to characterize large-scale WAM patterns during

97   the 1981-2019 period, which we subsequently stratify for days with MCS occurrence over SWA. This methodology

98   thus allows us to identify favourable types of large-scale environments driving the formation of MCSs within

99   different WAM stages.

100   The paper is organized as follows: Section 2 details the study area and data sources and how they were

101   processed. In section 3, the SOM methodology and other needed statistics used to investigate the relationship

102   between large-scale environment patterns and particular MCSs are presented. Section 4 discusses the main results,

103   which include the common features and different types of large-scale patterns associated with MCSs. Section 5

104   provides the summarized conclusions of the study.

105   **2 Data Sources and Processes**

106   **2.1 ERA5 Reanalysis Data and MCS Data**

107   The ECMWF fifth-generation atmospheric reanalysis (Hersbach et al., 2020), ERA5, was used as the main

108   product in this work. The dataset is generated using 41r2 of the Integrated Forecast System (IFS) model, based on a

109   four-dimensional variational data assimilation scheme, and takes advantage of 137 vertical levels and a horizontal

110   resolution of 0.28125° (31 km). The data provides hourly estimates of model integration. In this study, hourly zonal

111   and meridional winds (250 and 925 hPa), specific humidity (925 hPa), temperature (925 hPa), and convective

112 available potential energy (CAPE) in ERA5 during 1981–2020 were used to explore suitable large-scale

113 environments for the development of MCSs in SWA (5-9ºN, 10ºW-10ºE). The zonal and meridional wind, as well as

114 specific humidity at 925 hPa, are used to understand the penetration of monsoon flow inland. The zonal wind

115 difference between 925 hPa and 600 hPa is used as a shear change indicator while the temperature at 925 hPa is used

116 to visualize Saharan heat low (SHL) differences.

117 Twelve years of MCS snapshots (2004–15) detected from Meteosat Second Generation 10.8 μm-band

118 brightness temperatures (Schmetz et al. 2002, EUMETSAT 2021) are used to define MCS days in this study.

119 Following Klein et al. (2021), an MCS is defined here as a -50ºC contiguous cloud area larger than 5000 km^2. An

120 "MCS day" is then defined as a day with at least 5 MCS snapshots between 16 and 1900 UTC per day that is raining

121 >5mm within the SWA domain.

122

123 **3 Methodology**

124 **3.1 Self-organising Maps (SOMs) analysis**

125 The study uses the self organizing map (SOM; Kohonen 1982, 2001) technique to identify archetype

126 synoptic circulation patterns over the southern West Africa region by training a 9-node SOM with ERA5 daily 950

127 hPa geopotential height fields to produce 9 characteristic circulation patterns for the period 1981 to 2020. The

128 geopotential height circulation pattern is used here mainly based on its physically realistic output spanning a range

129 of circulation features found in the atmosphere (Hewitson and Crane, 2002). The SOM is a clustering technique that

130 is topologically sensitive and uses an unsupervised training method to cluster the training data (Lennard and Hegerl,

131 2014; Quagraine et al. 2019). It is preferred over other clustering methods such as the principal component analysis

132 (PCA) or K-means because the data is not discretized and orthogonality is not forced but rather treats the data as a

133 continuum (Reusch et al. 2005; Lennard and Hegerl, 2014). The steps within the technique can be broadly grouped

134 into two stages, namely the training stage and the mapping stage. Earlier studies (e.g. Hewitson and Crane 2002;

135 Kim and Seo 2016; Lee 2017; Rousi et al. 2015; Sheridan and Lee 2012) have successfully used this technique in

136 synoptic climatology to effectively preserve relationships between weather states while giving outputs that are

137 readily understood and can be easily visualized as an array of classified patterns. These classified patterns help in

138 interpreting relationships between large-scale regional circulation patterns and local weather expressions and rainfall

139 extremes (Hewitson and Crane 1996; Cassano et al. 2015; Wolski et al. 2018). There is a trade-off when choosing

140 the size of the SOM, as this is dependent on the need to generalize circulation states for analyses or the need to

141 capture predominant spatial characteristics that affect the local climate. Thus, in this study, we have tested several

142 sizes of the SOM and have arrived at using a 9-node SOM. The 9-node SOM is a compromise on states not being

143 overly generalized while capturing the dominant spatial characteristics over the region.

144

145 **3.2 Large-scale WAM patterns on southern West Africa MCS days**

146 Based on the 9 different large-scale node patterns, we explore within-node large-scale conditions that

147 characterize MCS days in SWA. For examination of environmental conditions suitable for SWA MCS activity,

148 large-scale conditions were taken from hourly ERA5 reanalysis data sampled at 1200 UTC when the daily

149 convective activity is more representative of pre-convective atmospheric conditions (Klein et al. 2021). Pre-
150 convective conditions are considered in the study to reduce the effects of feedback from the MCSs on environmental
151 conditions (Song et al. 2019). Composites of ERA5 large-scale environmental variables (temperature, wind, specific
152 humidity, and CAPE) are created for all node days, and for MCS days within each SOM node. Finally, the anomaly
153 in large-scale patterns between MCS days and node mean conditions are computed to determine MCS-favourable
154 adjustments in large-scale patterns within each node. A two-sided Student's t-test is used to determine significant
155 differences between node climatologies and MCS-day sub-samples.

156   In addition to large-scale condition composites, we also sample pre-convective (1200 UTC) local
157 atmospheric conditions (ERA5), for each 1800 UTC MCS at the location of minimum cloud top temperature. We
158 only consider 1800 UTC MCSs for local condition sampling to avoid oversampling similar atmospheric states from
159 several MCS time steps. These conditions are compared to the node climatology conditions at the same locations,
160 allowing us to explore the difference in node climatology versus MCS day conditions at the specific locations where
161 MCSs occurred on respective days.

162

163 **4 Results**

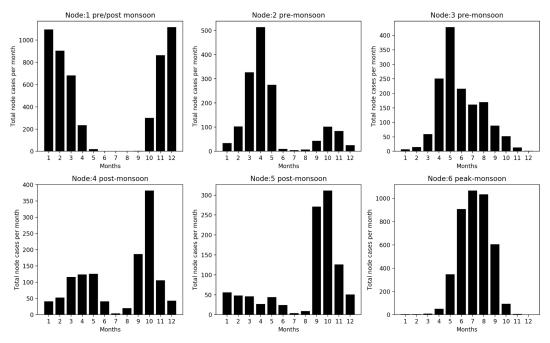164 **4.1 Node seasonality and mean conditions**

165   In analyzing the 9-node SOM (not shown), six SOM nodes (Fig. 1) with distinct synoptic states were
166 identified and were further associated with being either a pre-, post-, or peak-monsoon synoptic circulation type as a
167 result of which months in the year they dominantly occur. These nodes are hereafter referred to as nodes one (1) to
168 six (6). The SOM nodes are noted to generally represent patterns of the seasonal cycle. Circulation patterns in node
169 1 can be attributed to cases primarily observed in the first three months (January, February, and March) and the last
170 two months (November, and December), hence a pattern most representative of the dry season months. It is noted
171 that nodes 2 and 3 depict an environment that is prominent during the pre-monsoon season, with node 2 presenting a
172 clearer seasonal exclusivity while node 3 shows frequent occurrences throughout the monsoon season. Patterns of
173 node cases significant in the post-monsoon season are observed in nodes 4 and 5. However, node 4 evidently shows
174 transition patterns that have frequent occurrences in both pre and post-monsoon seasons although most prominent in
175 the post-monsoon season. Patterns in node 6 are more strongly related to peak monsoon conditions.

176

177

178

Figure 1. Monthly distribution of node cases based on SOM analysis

The SOMs classification of different synoptic states was based on 925hPa geopotential heights, with resulting patterns shown in Fig. 2. The patterns clearly show the signature of the well-known West African Heat Low (e.g. Lavaysse et al. 2009) moving northwards, strengthening over the course of the annual WAM cycle (from nodes 1, 2 and 3) and peaking in August, evident as an area of high pressure over the Sahara in node 6. Nodes 4 and 5 show stages of the weakening of the heat low post-monsoon, coinciding with a southward movement of the 650hPa high pressure area and linked southward retreat of mid-level easterly winds compared to node 6.

Figure 2. Composites of 925-hPa geopotential height (shading; gpm) and 650-hPa winds (vectors; m s^{-1}) in six nodes based on SOM analysis.
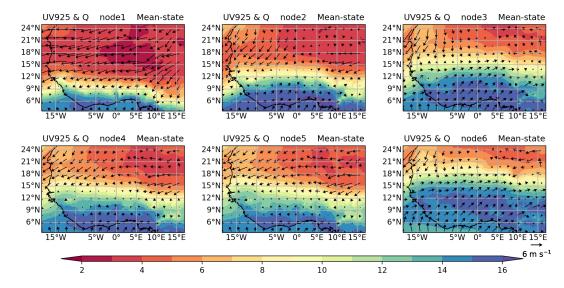
We now examine surface winds and moisture flows to explore their behaviour under the six distinct circulation types identified (Fig. 3). In the first node, the north-easterly winds dominate most of West Africa, with weak southerlies over SWA. This pattern in moisture distribution is evident in the dry season over West Africa, signaling a low moisture presence. The enhanced moisture observed in coastal areas of SWA can be attributed to the penetration of southerly winds. In pre-monsoon node 2, the southerly winds strengthen and move inland, causing the north-easterly winds to retreat. A similar effect is observed in nodes 3, 4, and 5 where the north-easterlies become weaker. In node 6, the south-westerlies are much more strengthened and move inland, further enhancing moisture flow from the South Atlantic towards the land, representative of peak monsoon flow. Wind patterns for low- and mid-levels (Figs. 2 and 3) illustrate vertically-sheared conditions coinciding with regions of high low-level specific humidity in all nodes (purple in Fig. 3), thus marking regions where atmospheric conditions may allow MCS development.

Weather and
Climate Dynamics
Discussions

207

Figure 3. Composites of specific humidity (shading; g kg^{-1}) and 925-hPa winds (vectors; m s^{-1}) in six nodes based on SOM analysis.

A further investigation into potential node frequency trends since the 1980s was conducted to ascertain whether certain node frequencies have changed over recent years (Fig. 4). No clear node frequency changes are observed during nodes associated with the dry and the monsoon seasons (node 1, 6). It is also striking that the two nodes associated with the second rainy season months (node 4, 5) show significant changes over the last 4 decades, indicating that this season may have been affected by long-term changes in the large-scale environment, although node 5 recovered in the last few years. But it would have to be investigated in more detail when exactly these trends occur and which variables are affected, which is out of scope of this study.
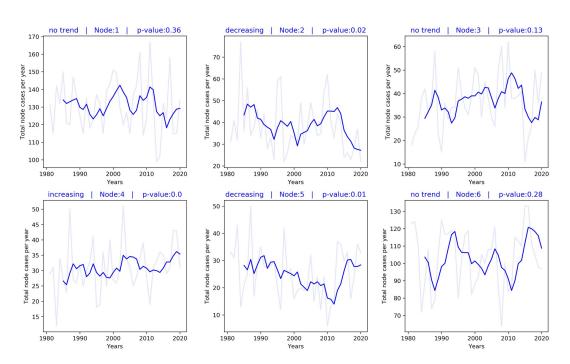
219

Figure 4. Time series of node frequency trends for node climatologies over the years. Deep blue line indicates 5-year rolling mean of node frequencies. The titles show the mann kendall trend test and the p-value for test of significance.
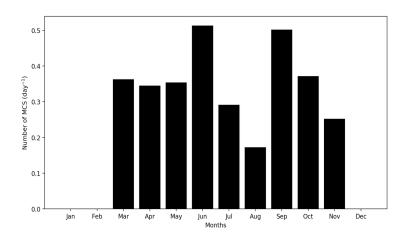
4.2 Large-scale conditions favouring MCS days

The environmental conditions favouring MCS occurrence are described in this section. Firstly, the monthly climatology of MCS frequency as captured by our MCS snapshots (average number of MCSs at 1800 UTC across SWA domain) is considered with a focus on rainfall months. A pronounced annual cycle of MCS numbers with frequency peaks in June and September is observed (Fig. 5). These peak months are associated with maximum rainfall during the major and minor rainy seasons across SWA respectively. The monthly climatology of MCS frequency decreases from June to August, with August being the local minimum. This local minimum corresponds to the so-called "little dry season" (Le Barbé et al., 2002; Vollmert et al., 2003) that exists before the southward retreat of the rainbelt.

9   9

Figure 5. Average annual cycle of MCSs at 1800 UTC within the SWA box showing the monthly average of MCS
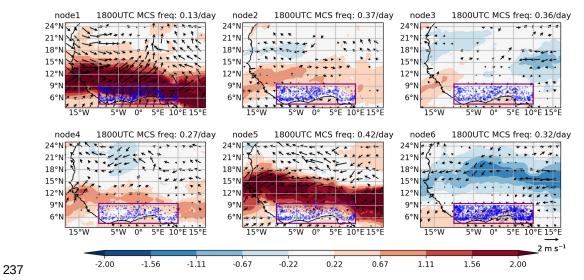number per day.

Figure 6. MCS-day composite anomalies of specific humidity (shading; g kg^{-1}) and 925-hPa winds (vectors; m s^{-1})
in six nodes based on SOM analysis. The purple box depicts the SWA region (5º–9ºN, 10ºW–10ºE) and the blue dots
indicate the location of MCSs during node days. Specific humidity anomalies are shown when they are significant at
the 5% level; wind vectors are shown when either the zonal or meridional wind anomalies are significant at the 5%
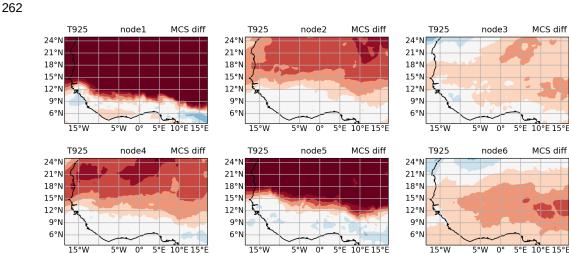level.

244   We consider the spatial distribution of large-scale environments associated with MCSs for each node over
245   the SWA region. In node 1, a positive widespread moisture anomaly maximum is observed with anomalous south-
246   westerly winds over SWA (Fig. 6). This depicts a substantial enhancement in the low-level moisture transport
247   during days of convective activities. In nodes 2, 3, 4, and 5, low-level moisture anomalies during convective activity
248   days show insignificant behaviour along the SWA coast. In node 5, a positive moisture anomaly is located over the
249   northern part of SWA. In node 6, a notable region of anomalous easterly winds coincides with negative moisture
250   anomalies over the Sahel. Strong easterly winds during MCS days reduce the moisture over the Sahel but introduce
251   more moisture over the coast. Comparing daily MCS frequencies, we find that MCSs are most likely to develop
252   under node 5 conditions featuring a northward-displaced moisture anomaly (0.42 MCSs per day), linked to
253   strengthened low-level westerlies. Given this node occurs predominantly from September and into November - the
254   minor rainy season in SWA (cf. Fig.~1), these patterns may in some cases be representative of a delayed monsoon
255   retreat.
256   Figure 7 shows a widespread increase in temperature north of SWA during days with active convection in
257   nodes 1, 2, 4, and 5. The SWA region itself reveals a negative and/or insignificant change in temperature during
258   MCS days when compared with the mean climatology. This could be a result of the presence of enhanced moisture
259   migrating from the Atlantic ocean inland (Fig. 6). Indeed, for nodes 1 and 5 this coincides with low-level westerly
260   wind south of 15N (cf. Fig. 6). In node 6, temperatures are enhanced in most parts of West Africa including SWA.
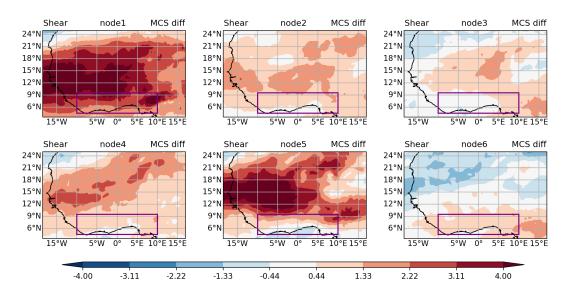261
262

263

264   **Figure 7.** Composite anomalies of 925hPa temperatures (°C) in six nodes based on SOM analysis. Temperature
265   anomalies are shown when they are significant at the 5% level.

266

267   Figure 8 shows the spatial distribution of wind shear anomaly between days with convective MCSs over
268   SWA and the climatological shear mean for the 6 different nodes across West Africa. Generally, all nodes except
269   node 6, reveal a widespread increase in shear anomaly over West Africa with nodes 1 and 5 depicting stronger
270   events. Wind shear tends to be stronger during the dry and early part of the major rainy season (node 1) with its peak
271   partly over SWA, but resides to the north of SWA during the minor rainy season (nodes 4 and 5), in line with
272   previously identified shear seasonality for the region (Klein et al. 2021). Nodes 4 and 5 (post-monsoon) however
273   still experience an appreciably significant increase in shear over SWA for MCS days during the minor rainy season.
274   Node 6 on the other hand, observes a significant increase in wind shear mainly confined to SWA. In line with the
275   expected shear response to an increased large-scale meridional temperature gradient, we find strongest shear
276   anomalies for nodes with strongest low-level temperature anomalies to the north of SWA (nodes 1,5; followed by
277   nodes 2,4), highlighting that a warmer Sahel can promote MCS-favourable conditions in SWA, particularly in the
278   pre- and post-monsoon seasons. Overall, these significant positive zonal shear anomalies for MCS days across all
279   nodes illustrate the importance of shear for MCS development in SWA throughout the year.

280
281

Figure 8. Composite anomalies of wind shear (m s^{-1}) in six nodes based on SOM analysis. Shear anomalies are
shown when they are significant at the 5% level.

285

286   Investigating the first order condition for convection development, we also evaluate CAPE for a parcel at
287   925 hPa to ascertain the level of increased MCS-day instability in various nodes over SWA (Fig. 9). A large strip of
288   higher CAPE values extending over the entire region of SWA and the southern Sahel from 5°N−15°N is observed
289   (node 1). This large strip of higher CAPE is situated further north of SWA for node 5, while part of the western
290   coast tends to observe patterns of lower CAPE values, suggesting increased MCS likelihood only for eastern parts of

291 the domain. Node 3 shows a swath of high CAPE values in particular to the east and in some instances extends to

292 the central (node 4) and south-western parts of SWA (node 6). For nodes 3-6, higher CAPE conditions over SWA

293 are to differing degrees significantly associated with decreased CAPE in the Sahelian region, creating a dipole

294 pattern that can occur during pre-, peak- and post-monsoon periods according to node frequencies (cf. Fig 1).

295 Overall, all nodes show positive CAPE anomalies for MCS-days in parts of SWA, creating an environment

296 sufficiently unstable to support the development of convection. It can be said that regions over SWA that exhibit a

297 higher CAPE on MCS days also depict stronger shear (Fig. 8). Indeed, it has previously been shown that colder,

298 more intense MCSs predominantly occur under conditions with high CAPE and high shear anomalies (Klein et al,

299 2021), which we show is consistent across all classified large scale patterns.
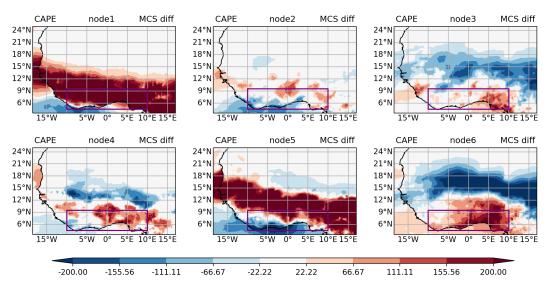
300

301

302

303 **Figure 9.** Composite anomalies of CAPE (J kg $^{-1}$) for MCSs occurring in each type of large-scale environment

304 determined by the SOM analysis over SWA. CAPE anomalies are shown when they are significant at the 5% level.
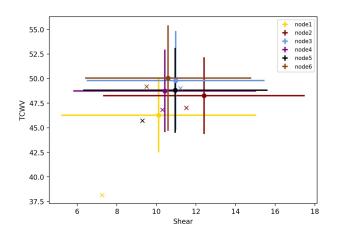
305

306 **4.3 MCS driver variability within nodes**

307 The drivers of MCSs within different nodes are considered to examine their relative importance within the different

308 large-scale states (Fig. 10), concentrating on total column water vapor (TCWV) and zonal wind shear. Node 1

309 climatological conditions depict both, a very low initial shear and TCWV, illustrating the relatively storm-hostile

310 mean conditions for this node, predominantly representing dry season conditions and explaining the low storm

311 frequency of only 0.13 per day (cf. Fig. 6). Interestingly, on storm days, conditions for this node shift to within the

312 range of environmental conditions identified for other nodes with higher storm frequencies, albeit node 6 MCS-day

313 conditions still represent the lowest values in TCWV and shear.

314

Figure 10. Mean MCS conditions over SWA for the different nodes. Dots show the mean within 1 standard deviation (whiskers) across each node. The symbol (x) denotes the mean environmental condition for all node days (MCS and non-MCS).

Pre-monsoon nodes (nodes 2 and 3) observe initial higher shear conditions than all other nodes with appreciably higher TCWV. Node 2 observes an increase in shear (about 1 m/s) and also a bit more TCWV. Not much change is observed in the shear and TCWV value for node 3, making node 2 the season with relatively strong instability since this node (node 2). Comparing nodes 4 and 5 (both post-monsoon nodes), it can be observed that node 5 has lower shear to start with and thus needs higher shear change to produce MCS conditions very similar to node 4. Node 4 on the other hand shows mostly TCWV change but has a bit more shear so, in spite of the smaller shear anomaly (Fig. 8), the resulting MCS conditions are rather similar. Node 6 depicts an initial environmental condition of high TCWV over SWA, which is typical of periods with frequent convective activities during peak monsoon. During MCS events, there is a slight increase in shear (about 1 m/s) and TCWV (about 0.8 kg/m^2), depicting more convective activities during this season.

Generally, it can be noted that all nodes show increased TCWV on MCS days compared to their climatology. The smallest changes for both TCWV and shear between climatology and MCS day occur for node 3, which shows the highest frequency for pre-monsoon transition month May but is still common throughout the monsoon season (c.f. Fig. 1) . Together with node 4, it is also the only node for which shear conditions remain approximately similar, but with climatological shear strengths already reaching > 10 m /s at MCS location. Overall, node environmental conditions become more similar for MCS-days relative to the climatologies, illustrating that favourable MCS conditions converge towards high TCWV (affecting CAPE), and high shear environments irrespective of the large-scale situation.

339   **5 Conclusion**

340   The study identified six synoptic states (pure node analysis) and then examined what changes are
341   associated with favourable MCS environments in Southern West Africa under these states. For the definition of
342   synoptic states and MCS days, we used self-organizing maps (SOM) based on ERA5 geopotential height data and
343   12 years of tracked MCSs using Meteosat Second Generation (MSG) 10.8 μm-band brightness temperature data
344   (2004-15), respectively. The identified synoptic states based on the SOM nodes are noted to generally represent
345   patterns of the seasonal rainfall cycle. Circulation patterns in node 1 can be attributed to cases primarily observed in
346   the dry season months (January, February, November, and December). An environment representative of the pre-
347   monsoon season is depicted by nodes 2 and 3, with node 2 presenting a clearer seasonal exclusivity. Patterns of the
348   post-monsoon season are observed in nodes 4 and 5 with node 4 evidently depicting transition patterns that have
349   frequent occurrences in both pre and post-monsoon seasons although prominent in the post-monsoon season. Peak
350   monsoon conditions are clearly represented in node 6 with large-scale conditions occurring mainly in June, July, and
351   August. The south-westerly winds observed over SWA are strengthened and move inland, enhancing moisture flow
352   from the South Atlantic towards the land during the peak monsoon. In the pre-monsoon and post-monsoon seasons,
353   similar but weakened south-westerly circulation patterns are observed. The synoptic-state-related MCSs realize a
354   pronounced annual cycle of MCS numbers with frequency peaks in June and September. These peak months are
355   well associated with maximum rainfall during the major and minor rainy seasons across SWA respectively. During
356   the course of the year, MCSs are most likely to develop under post-monsoon conditions featuring a northward-
357   displaced moisture anomaly (0.42 MCSs per day) which is associated with strengthened low-level westerlies, and in
358   some cases may be representative of a delayed monsoon retreat. Furthermore, the strongest shear anomalies over
359   SWA are realized in seasons with the strongest low-level temperature anomalies to the north of SWA, representative
360   of favourable MCS conditions in SWA during periods of a warmer Sahel. Regions over SWA that show stronger
361   shear on MCS days also depict higher CAPE. We found node environmental conditions to become more similar for
362   MCS-days relative to the node climatologies, illustrating that favourable MCS conditions converge towards high
363   TCWV/high shear states. Overall, our results show that MCSs develop on average in similar high moisture, high
364   shear local environments under all large-scale situations throughout the year. The latter however defines the
365   frequency at which favourable MCS environments can occur.

366

367   *Code and data availability*. Codes for the findings of this study are available upon reasonable request from the
368   authors. The processing of ERA5 data made direct access to the primary data archive held at ECMWF, and is
369   available from the Copernicus Data Store (https://cds.climate.copernicus.eu/) and the MSG data are available from
370   http://www.eumetsat.int.

371

372   *Author contributions*. FN, NABK and CK conceptualized the study, with input from KAQ; All authors contributed
373   to and discussed the methodological design, and analyses were conducted by FN and CK; FN, ROB and KAQ wrote
374   the manuscript draft; CK, NABK, PE, GMLDQ and HAK reviewed and edited the manuscript.

375

382   **References**

383   Augustin, D., Pascal, I. M., Jores, T. K., Elisabeth, F. D., Cesar, M. B., Michael, T. F., ... & Firmin, B. A. (2022).
384   Impact assessment of the West African monsoon on convective precipitations over the far north region of
385   Cameroon. Advances in Space Research.

387   Baidu, M., Schwendike, J., Marsham, J. H., & Bain, C. (2022). Effects of vertical wind shear on
388   intensities of mesoscale convective systems over West and Central Africa. Atmospheric Science Letters, e1094.

390   Bisselink, B., Zambrano-Bigiarini, M., Burek, P., & De Roo, A. (2016). Assessing the role of uncertain precipitation
391   estimates on the robustness of hydrological model parameters under highly variable climate conditions. Journal of
392   Hydrology: Regional Studies, 8, 112-129.

394   Cassano, E. N., J. M. Glisan, J. J. Cassano, W. J. Gutowski, and M. W. Seefeldt, 2015: Self-organizing map analysis
395   of widespread temperature extremes in Alaska and Canada. Climate Res., 62, 199–218,
396   https://doi.org/10.3354/cr01274

398   Chen, Y., Luo, Y., & Liu, B. (2022). General features and synoptic-scale environments of mesoscale convective
399   systems over South China during the 2013–2017 pre-summer rainy seasons. Atmospheric Research, 266, 105954.

401   Feng, Z., Leung, L. R., Liu, N., Wang, J., Houze Jr, R. A., Li, J., ... & Guo, J. (2021). A global high-resolution
402   mesoscale convective system database using satellite-derived cloud tops, surface precipitation, and tracking. Journal
403   of Geophysical Research: Atmospheres,126(8), e2020JD034202.

405   Guo, Y., Du, Y., Lu, R., Feng, X., Li, J., Zhang, Y., & Mai, Z. (2022). The characteristics of mesoscale convective
406   systems generated over the Yunnan-Guizhou Plateau during the warm seasons. International Journal of Climatology.

408   Hersbach, H., Bell, B., Berrisford, P., Hirahara, S., Horányi, A., Muñoz-Sabater, J., Nicolas, J., Peubey, C., Radu,
409   R., Schepers, D., et al. (2020). The era5 global reanalysis. Quarterly Journal of the Royal Meteorological Society,
410   146(730):1999-2049.

411

412   Hewitson, B., and R. Crane, 1996: Climate downscaling: Techniques and application. Climate Res., 7, 85-95,
413   https://doi.org/10.3354/cr007085.

414

415   Hewitson, B., and R. Crane, 2002: Self-organizing maps: Application to synoptic climatology. Climate Res., 22, 13-
416   26, https://doi.org/10.3354/cr022013.

417

418   Houze Jr, R. A. (2004). Mesoscale convective systems. Reviews of Geophysics, 42(4).

419

420   Kim, H. K., and K. H. Seo, 2016: Cluster analysis of tropical cyclone tracks over the western North Pacific using a
421   self-organizing map. J. Climate, 29, 3731–3751, https://doi.org/10.1175/JCLI-D-15-0380.1.

422

423   Klein, C., Nkrumah, F., Taylor, C. M., & Adefisan, E. A. (2021). Seasonality and trends of drivers of mesoscale
424   convective systems in southern West Africa. Journal of Climate, 34(1), 71-87.

425

426   Kohonen, T., 1982: Self-organized formation of topologically correct feature maps. Biol. Cybern., 43, 59–69,
427   https://doi.org/10.1007/BF00337288.

428

429   Kohonen, T., 2001: Self-Organizing Maps. Springer, 502 pp.

430

431   Kusangaya, S., Warburton, M. L., Van Garderen, E. A., & Jewitt, G. P. (2014). Impacts of climate change on water
432   resources in southern Africa: A review. Physics and Chemistry of the Earth, Parts a/b/c, 67, 47-54.

433

434   Lavaysse, C., Flamant, C., Janicot, S., Parker, D. J., Lafore, J. P., Sultan, B. and Pelon, J.: Seasonal evolution of the
435   West African heat low: A climatological perspective, Clim. Dyn., 33(2–3), 313–330, doi:10.1007/s00382-009-0553-
436   4, 2009.

437

438   Lee, C. C., 2017: Reanalysing the impacts of atmospheric teleconnections on cold-season weather using multivariate
439   surface weather types and self-organizing maps. Int. J. Climatol., 37,
440   3714–3730, https://doi.org/10.1002/joc.4950.

441

442   Lennard, C., and G. C. Hegerl, 2014: Relating changes in synoptic circulation to the surface rainfall response using
443   self-organizing maps. Climate Dyn., 44, 861–879, https://doi.org/10.1007/s00382-014-2169-6.

444

445   Li, P., Moseley, C., Prein, A. F., Chen, H., Li, J., Furtado, K., & Zhou, T. (2020). Mesoscale convective system
446   precipitation characteristics over East Asia. Part I: Regional differences and seasonal variations. Journal of Climate,
447   33(21), 9271-9286.

448

449   Maidment, R. I., Grimes, D., Allan, R. P., Tarnavsky, E., Stringer, M., Hewison, T., ... & Black, E. (2014). The 30
450   year TAMSAT African rainfall climatology and time series (TARCAT) data set. Journal of Geophysical Research:
451   Atmospheres, 119(18), 10-619.

452

453   Maranan, M., Fink, A. H., & Knippertz, P. (2018). Rainfall types over southern West Africa: Objective
454   identification, climatology and synoptic environment. Quarterly Journal of the Royal Meteorological Society,
455   144(714), 1628-1648.

456

457   Nesbitt, S. W., Cifelli, R., & Rutledge, S. A. (2006). Storm morphology and rainfall characteristics of TRMM
458   precipitation features. Monthly Weather Review, 134(10), 2702-2721.

459

460   Quagraine, K. A., B. Hewitson, C. Jack, I. Pinto, and C. Lennard, 2019: A methodological approach to assess the co-
461   behavior of climate processes over southern Africa. J. Climate, 32, 2483–2495, https://doi.org/10.1175/JCLI-D-18-
462   0689.1

463

464   Sheridan, S., and C. C. Lee, 2012: Synoptic climatology and the analysis of atmospheric teleconnections. Prog.
465   Phys. Geogr., 36, 548–557, https://doi.org/10.1177/0309133312447935.

466

467   Thorncroft, C. D., Nguyen, H., Zhang, C. and Peyrille, P., 2011: Annual cycle of the West African monsoon:
468   Regional circulations and associated water vapour transport, Q. J. R. Meteorol. Soc., 137(654), 129–147,
469   doi:10.1002/qj.728.

470

471   Wolski, P., C. Jack, M. Tadross, L. van Aardenne, and C. Lennard, 2018: Interannual rainfall variability and SOM-
472   based circulation classification. Climate Dyn., 50, 479–492, https://doi.org/10.1007/s00382-017-3621-1.

473
474
475
476
477
478
479
480
481
482
483
484